Enhanced Magnetic Field Sensing Using a Magnetic Graphene Oxide-Coated Tapered Fiber Optic Sensor

Qianyun Yin, Ragini Singh, Bingyuan Zhang, and Santosh Kumar, *Senior Member, IEEE*

***Abstract*—In this work, we have developed a portable fiber-optic sensor characterized by its robust immunity to electromagnetic interference (EMI), exceptional sensitivity, and real-time monitoring capabilities for magnetic fields. This sensor exhibits remarkable accuracy and stability in measuring both increasing and decreasing magnetic fields. To enhance the sensor's performance, we designed, simulated, and fabricated a tapered fiber structure with a tapered diameter of 40 μm using a combiner manufacturing system (CMS). Additionally, we employed a 2-D material known as magnetic graphene oxide (MGO) to immobilize the sensing region of the tapered fiber optic sensor. The key principle behind this sensor lies in the refractive index (RI) changes of MGO when subjected to a magnetic field, leading to a wavelength shift in the transmitted spectrum. Through rigorous experimentation, we thoroughly assessed the measurement range, sensitivity, and accuracy of the sensor in detecting both increasing and decreasing magnetic fields. Consequently, we determined the sensitivity of the fiber optic magnetic field sensor to be 0.9 and 1.6 pm/mT for increasing and decreasing magnetic fields in the wide measurement range of 5–600 mT, respectively. This sensor holds significant promise in various applications, including medical testing and scientific measurements, owing to its exceptional accuracy, compact size, and noninvasive measurement capabilities. Furthermore, its stability and noncontact measurement feature position it as a valuable tool in controlled nuclear fusion, space exploration, and geophysical research.**

***Index Terms*—Magnetic field sensor, magnetic graphene oxide (MGO), magnetometer, optical fiber sensor, tapered fiber structure.**
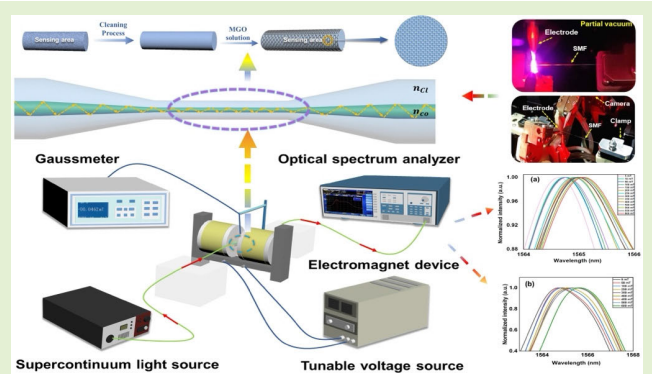
Qianyun Yin and Bingyuan Zhang are with the Ji Xianlin College and the School of Physics Science and Information Technology, Liaocheng University, Liaocheng 252059, China (e-mail: 2316334238@qq.com; zhangbingyuan@lcu.edu.cn).

Ragini Singh is with the College of Agronomy, Liaocheng University, Liaocheng 252059, China (e-mail: singh@lcu.edu.cn).

Santosh Kumar is with the Shandong Key Laboratory of Optical Communication Science and Technology, School of Physics Science and Information Technology, Liaocheng University, Liaocheng 252059, China, and also with the Department of Electronics and Communication Engineering, K. L. Deemed to be University, Guntur, Andhra Pradesh 522302, India (e-mail: santosh@lcu.edu.cn).

I. INTRODUCTION

MAGNETIC field sensors have been used in a wide range of scientific and industrial measurements in a variety of fields, including gas field exploration logging and production logging [1], military [2], navigation [3], [4], biomedical detection [5], [6], [7], [8], [9], aerospace industry [10], space and geophysical research, and controlled nuclear fusion [11], [12]. Conventional electrical magnetic field sensors mainly rely on the self-inductance and mutual inductance of coils to achieve magnetic field measurements [13], [14], which leads to the shortcomings of conventional electrical magnetic field sensors such as low-frequency response, difficulty in real-time dynamic measurements, susceptibility to electromagnetic interference (EMI), and the resolution of the magnetic field sensors is greatly affected by the range of magnetic field measurements. Due to its small size, low sensitivity to external influences, high resistance to EMI, and ease of real-time dynamic measurements, the fiber optic magnetic field sensor used in this study is more advantageous in the field of magnetic field detection. For the development of
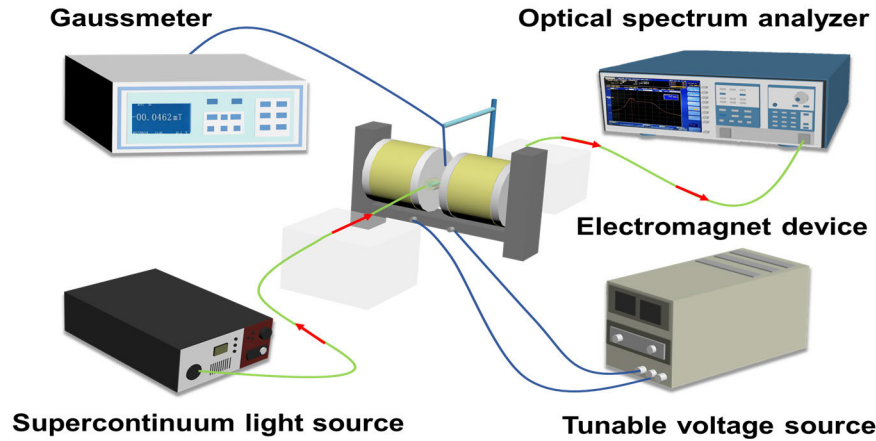
Fig. 1. Experimental setup for measuring magnetic field.

conventional fiber optic magnetic field sensors, magnetic fluids of ferromagnetic materials were used as sensing elements. Over time, the magnetic fluid deposits and forms a layer that is difficult to disperse, reducing the reusability of the fiber optic sensor [6]. In addition, oxidation and separation of particles, agglomeration effects, and stability are the primary issues that must be addressed during the optimization of magnetic fluid-based probes [6]. Due to its magnetic and electrical properties, high specific surface area, unique catalytic ability, and numerous applications, magnetic graphene oxide (MGO) has garnered considerable interest [15]. Under laboratory conditions, MGO has excellent stability, is simple to synthesize and functionalize, is easily separated by magnetism, possesses low toxicity and is inexpensive [16]. In this experiment, we designed and developed an unique magnetic field sensor with a tapered fiber optic structure and a sensing element comprised of MGO on a tapered area. Modifying the current to the electromagnet, varies the strength of the magnetic field surrounding the probe. As the magnetic field varies, the magnetic domains cause a change in the refractive index (RI) of the sensing layer, that results in a change in the modal properties of the light propagating along the fiber and a displacement of the wavelength [17].

The purpose of this experiment is to simulate and conduct an in-depth analysis of the distribution of the evanescent field of the tapered optical fiber structure that helps to achieve miniaturization, robustness, portability, economy, and practicality. In the design and fabrication of the fiber optic probe, combiner manufacturing system (CMS) was used to process the tapered fiber optic structure, and the fusion-drawing method was utilized to obtain a 40 μm tapered fiber optic structure. During the experiment, the magnetic field around the probe is altered by varying the current of the tunable voltage source, and the magnetic field in the fiber optic sensing region is measured with a Gaussmeter, allowing for real-time monitoring of the magnetic field in industry of space and geophysical research, and controlled nuclear fusion.

II. EXPERIMENTAL SECTION

A. Measurement and Instrument

In this experiment, the experimental setup used to characterize the probe's sensing properties is depicted in Fig. 1.

Single-mode fiber (SMF) is the main structure of the sensor, purchased from Shenzhen EB-Link Technology Company China. The experimental setup consists of a supercontinuum spectral light source (SUPERK COMPACT, NKT Photonics, 450–2400 nm), an optical spectrum analyzer (OSA, AQ6370D, YOKOGAWA, 600–1700 nm), a Gaussmeter (CH-1800, CH-Magnetoelectricity Technology), an electromagnet (Shanghai Huayan Instrument Company) for generating the magnetic field, and a voltage source with adjustable output. In this experiment, two vertical supports ensured that the sensing portion of the probe was always positioned in the center of the magnetic field generator. The effect of temperature on magnetic field measurement was eliminated, and all experiments were performed at room temperature. During the experiment, the magnetic field surrounding the probe can be altered by means of a tunable voltage source, where an increasing magnetic field can be obtained by increasing the voltage and a decreasing magnetic field can be obtained by decreasing the voltage. During the process of adjusting the magnetic field by varying the voltage, the changing magnetic field was monitored in real-time using a Gaussmeter, and the spectral changes caused by the changing magnetic field were recorded using an OSA. When magnetic field measurements are performed using tapered fiber optic structures coated with MGO, the effect of the concentration of MGO on the sensitivity of the probe must be taken into account. This is because denser magnetohydrodynamic deposition on thicker nanostranded layers results in total absorption of cladding modes of higher order [18].

B. Sensing Principle

When magnetic field (H) is applied to MGO, its dielectric magnetization (χ_e) changes, which alters the corresponding RI (n_{MF}). The following relationship exists between the RI of the MGO and the RI [18]:

$$\eta_{MGO} = \sqrt{\epsilon_{MGO}} = \sqrt{1 + \chi_e}. \tag{1}$$

This experiment's optical fiber consists of a core and cladding with different RIs. When light propagates to the core region, a portion of the light will form an evanescent wave (EW) within the cladding. The penetration depth of the EW
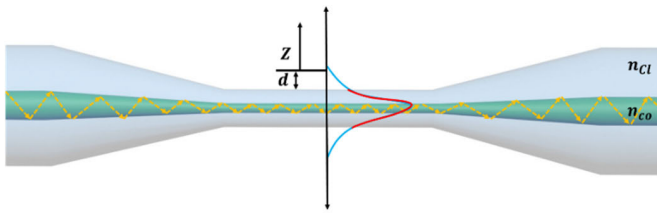
Fig. 2. Optical signal propagation through tapered optical fiber structure.
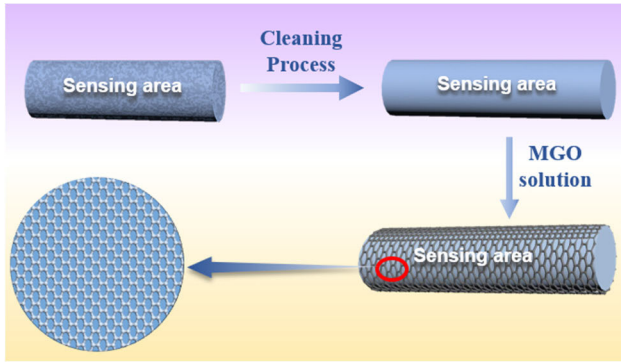
Fig. 3. Process of MGO coating over tapered optical fiber.

in the cladding is expressed as [19]

$$d_p = \frac{\lambda}{2\pi\sqrt{n_{co}^2\sin^2\theta_i - n_{cl}^2}}. \tag{2}$$

As shown in Fig. 2, the light intensity of a EW decreases exponentially along the z-axis of the fiber, as denoted by the expression [20]

$$I_z = I_0 e^{-\frac{d}{z}}. \tag{3}$$

In this experiment, the conventional tapered optical fiber was optimized to improve the optical fiber's sensing performance by coating its surface with MGO, as depicted in Fig. 3. When light is incident on nanoparticles composed of the row of graphene oxide, and the photon frequency matches the overall vibrational frequency of the nanoparticle's conduction electrons, then MGO absorbs the photon energy strongly, thereby significantly enhancing the sensing performance.

C. Simulation of Sensor Probe

This experiment is simulated using the beam propagation method (BPM) algorithm in RSoft. First, the simulation model was built using RSoft computer-aided design (CAD), and it is worth noting that the parameters used in the simulation model building process are exactly the same as the tapered fiber structure used in this experiment. An ordinary SMF has a length of 2300 μm, a diameter of 125 μm, and a core diameter of 8.2 μm, as shown in Fig. 4.

The length of the fiber tapered area is 2300 μm and the diameter is 40 μm. The RIs of the fiber core and cladding are 1.4504 and 1.4447, respectively. In this case, background index of simulation model is 1. Finally, the light source type is set to the fundamental mode.
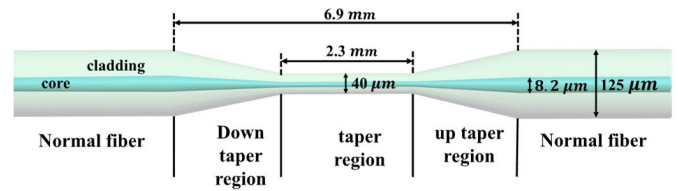
Fig. 4. Schematic of the tapered optical fiber structure.
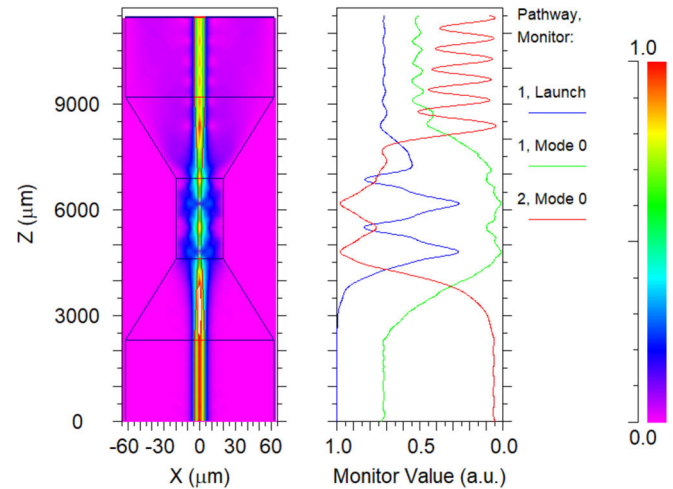
Fig. 5. Evanescent field analysis in tapered optical fiber structure.

Fig. 5 represents the simulation results of the tapered fiber structure using RSoft software. Here, 1, Launch represents the total energy distribution of the light source incident on the fiber core. 1, Mode 0 indicates the energy distribution of the propagating modes within the fiber core. 2, Mode 0 denotes the energy distribution of the propagating modes within the cladding. From Fig. 5, it can be seen that when the light passes through the tapered region of the optical fiber, the energy of the core mode decreases rapidly, while the energy of the cladding mode increases sharply, which makes the main propagation mode of the optical fiber in the tapered region change from the core propagation mode to the cladding propagation mode. At the same time, core modes and cladding modes are continuously coupled in the tapered region of the fiber, leading to excitations in the energy distribution in the sensing region. Simulation results show that the tapered fiber structure can excite strong cladding modes, and the structure is conducive to EW generation.

D. Fabrication of Sensing Probe

In this study, a CMS (3 SAE Technologies Inc., Franklin, TN, USA) was used to develop the highly repeatable SMF-based tapered fiber optic structure. During the fabrication of the tapered fiber optic structure, CMS is heated by a plasma heating system, during which the plasma temperature increases with the heating power and a "thermally stable plasma" is generated when a certain power is reached. This plasma is extremely thermally stable in a vacuum, and the thermal repeatability of thermally stabilized plasma in CMS is over ten times greater than that of existing arc technologies. These characteristics allow the CMS heating temperature to be unaffected by factors such as electrode aging or wear
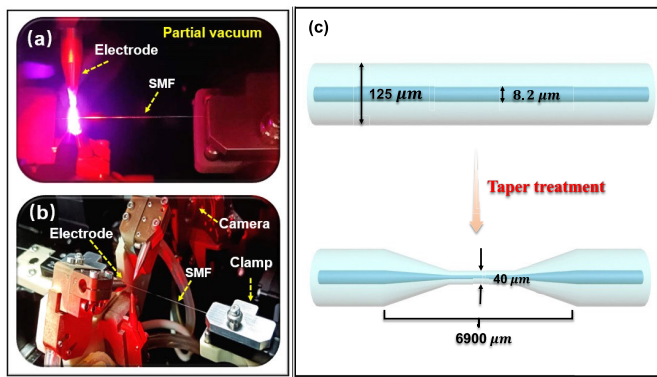
Fig. 6. (a) Internal structure of the CMS instrument, (b) three electrode heating process, and (c) taper optical fiber structure fabrication steps.

and tear, thereby enhancing the fiber fabrication process's efficiency and repeatability. Using CMS, the entire process of producing tapered fiber stricture can be managed by a well-tested computer program. Adjusting the initial power, the length of the taper area, the diameter of the taper, etc., can be performed multiple times during the production of the fibers in order to produce a repeatable taper structure. The use of CMS to develop new fiber optic structures is summarized below: First, the SMF's coating layer must be stripped and the fiber's surface must be cleaned with an ethanol solution. The cleaned fiber is then encapsulated in a fiber optic platform, where the CMS's vacuum control module produces a semivacuum environment around the SMF. As shown in Fig. 6(a), when the ambient vacuum inside the CMS reaches a predetermined value of 3, the three heating electrodes undergo a continuous and uniform discharge, as shown in Fig. 6(b). At the same time, the z-axis motor will move the fiber optic platform in the programmed direction, gradually increasing the diameter of the tapered region of the fiber structure to 40 μm and forming a complete tapered structure, as shown in Fig. 6(c). As shown in Fig. 6(b), the 2-D image of the taper fiber was scanned at the end of the tapering process using the internal inspection device of the CMS to ensure the uniformity of the fiber structure during the tapering process.

III. RESULTS AND DISCUSSIONS
A. Characterization of Nanomaterials

MGO is a compound that is composed of magnetic nanoparticles and GO with unique physicochemical properties such as nanometer size, large specific surface area, para-magnetism, and biocompatibility. Because it contains many oxygen-containing reactive groups, such as epoxy, carbonyl, and hydroxyl groups, it not only retains the basic framework of graphene, but also has higher bioactivity than graphene. At the same time, compared with graphene, MGO has the character-istics of high purity of graphene while having low production costs and easy mass production. MGO, as a superparamag-netic material, contains Fe_3O_4 magnetic nanoparticles inside, while retaining part of the original surface oxygen-containing functional groups of GO. Due to the dispersion of π-electrons and sp inside MGO, these π-electrons can move freely and align along the direction of the magnetic field, increasing the magnetic moment of MGO. In that work, we coated MGO on a tapered area as a sensing element. The magnetic field around
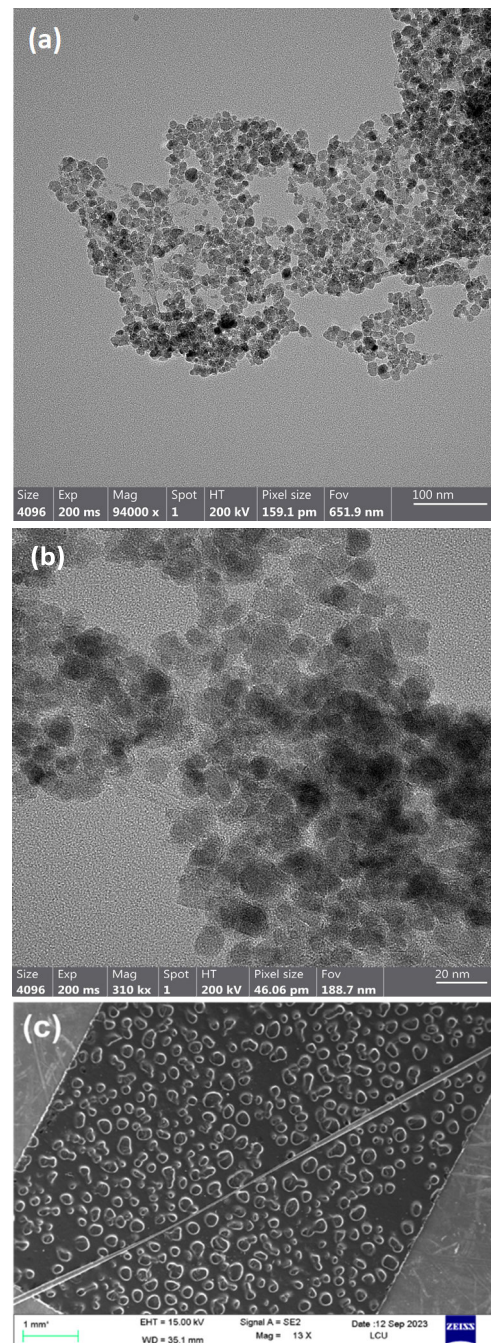
Fig. 7. HR-TEM image of MGO at different magnification (a) 94000X, (b) 310 KX, and (c) SEM image of bare tapered probe surface.

the probe varies with small changes in the electromagnet current. As the magnetic field changes, the magnetic domain phenomenon generated by the MGO causes a change in the RI of the sensing layer, which in turn causes a change in the modal properties of light propagating along the fiber. This phenomenon causes a shift in the peak wavelength.

By monitoring the change in peak wavelength, changes in the magnetic field in a small area around the probe can be detected [17]. In this experiment, MGO is an excellent choice as a probe coating material due to its excellent paramagnetic and magnetic properties [21]. The high-resolution transmission electron microscopy (HR-TEM) image of MGO at different magnification is shown in Fig. 7(a) 94000X and (b) 310 KX. The Fe and GO particles are especially visible in TEM images.

The MGO modification and distribution on the sensor are influenced by the surface topography of the sensor. The scanning electron microscopy (SEM) image of the developed tapered fiber probe is shown in Fig. 7(c). In the tapered region of this image, we can clearly see a symmetric straight tapering with a diameter of 40 μm. This implies that the MGO-modified sensing probe is a solid base for the subsequent measurement studies.

B. Optimization of Sensor Structure

In this experiment, three sets of 40 μm tapered fiber structures with the same diameter were fabricated using SMF and multimode fiber (MMF), respectively. The transmission spectra of the two types of fibers were measured. The results of these measurements are depicted in Fig. 8(a). These experimental results indicate that SMFs have better sensing performance than MMFs. In this experiment, the diameter of the tapered area has a significant impact on the properties of the tapered fiber structure. The sensitivity of the sensor diminishes as the taper region grows when the diameter exceeds the dispersion inflection point (8.75 μm) [22]. Therefore, we developed tapered fiber structures with diameters of 25, 40, 50, and 60 μm, respectively, and examined the transmission spectra of four groups of fibers of various diameters in order to choose the best fiber structure. According to Fig. 8(b), the measured findings demonstrate that when the tapered diameter is reduced, the output strength also drops. Strength loss is brought on by power leakage in the taper region, which can utilize to detect changes in the external RI. The taper fiber with a diameter of 25 μm has the lowest output strength, as can be seen from the Fig. 8(b). However, considering the practical value of the probe, the taper area with a diameter of 25 μm is fragile due to its small diameter, which is easy to damage during production and use, thereby increasing the difficulty of development and reducing the service life of the probe. Therefore, in this work, all sensor probes have a taper area with a diameter of 40 μm. Fig. 8(c) and (d) depicts the structural repeatability images for two sets of 40 μm tapered fiber structures composed of SMFs, demonstrating the high reproducibility of our prepared tapered fiber probes.

On the basis of the scanning diagram of the fiber structure, it is evident that the tapered fiber structure has excellent reproducibility, and that the tapered fiber structure we prepared matches the ideal tapered area diameter desired in the simulation experiments.

C. Characterization of Nanomaterials-Immobilized Structure

The morphology of the MGO coating on the surface of the optical fiber was observed with SEM. Fig. 9(a) shows the tapered optical fiber-based magnetic field sensor, and Fig. 9(b) shows the MGO over the tapered optical fiber structure. As shown in Fig. 9(b), the MGO is distributed uniformly on the surface of the tapered optical fiber.

D. Magnetic Field Measurement

Fig. 10 depicts the transmission spectra of this tapered fiber structure before and after coating it with MGO. Experiments
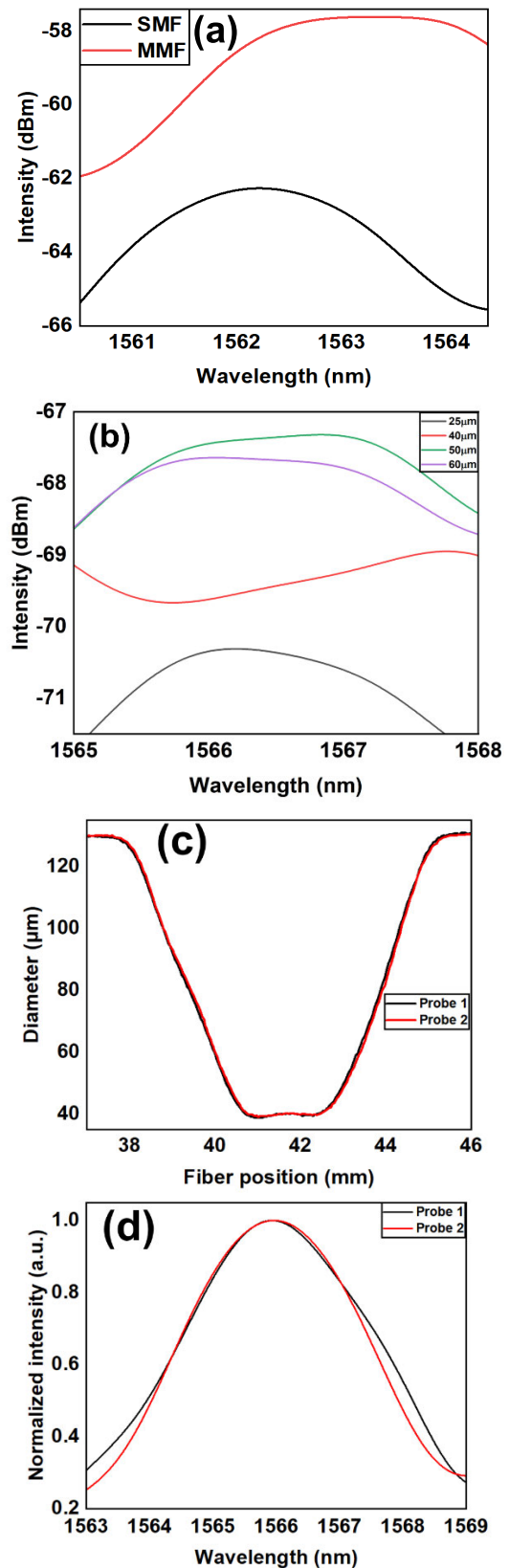
Fig. 8. (a) Intensity spectrum of SMF and MMF, (b) analysis of output transmitted intensity with different diameters of tapered fiber structures and repeatability analysis, (c) diameter scan result, and (d) normalized intensity spectrum of fabricated taper fiber structures.

demonstrate that the transmission intensity of light is higher for the MGO-coated tapered fiber structure, thereby enhancing the sensing ability. Comparing Figs. 11–13 show that
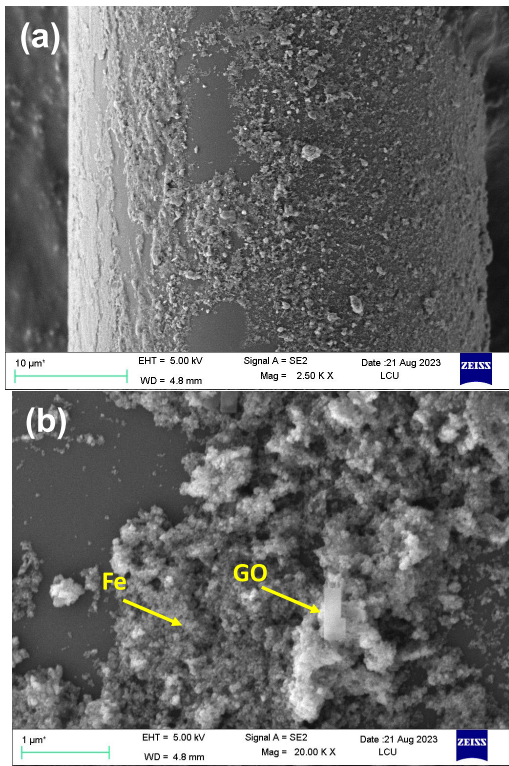
Fig. 9. (a) Tapered optical fiber-based magnetic field sensor and (b) MGO over the tapered optical fiber structure.
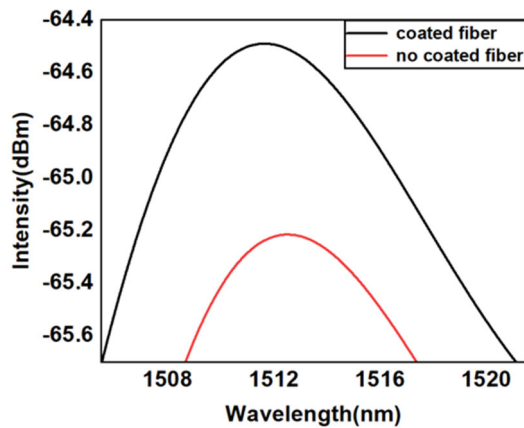
Fig. 10. Comparison of the spectral characteristics of MGO-coated and uncoated tapered fiber structures.

Fig. 11. Magnetic field detection using an uncoated taper fiber sensor.
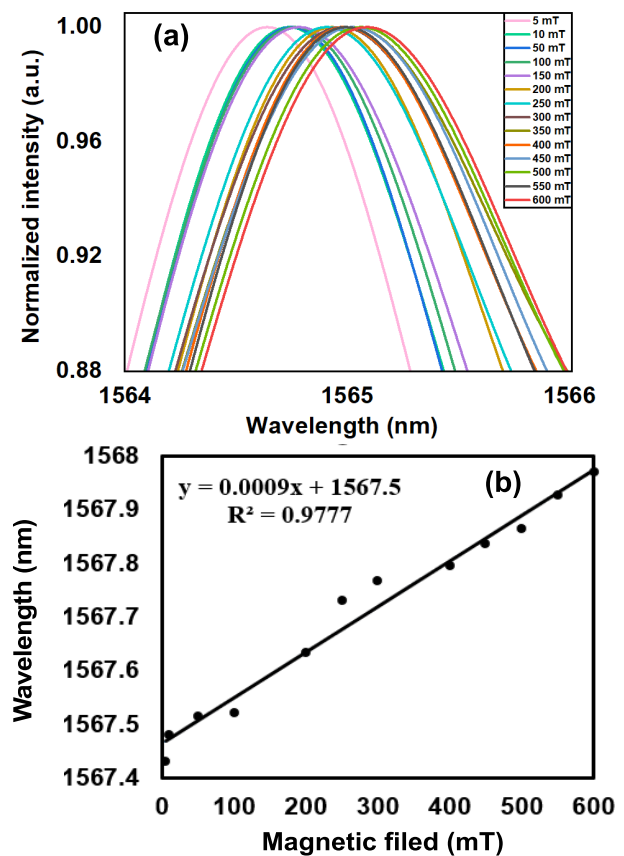
Fig. 12. Measurement of the magnetic field (during forward sensing) using the proposed SMF-based MGO-coated tapered fiber structure (a) sensing spectrum and (b) linear plot of the proposed sensor.

the optimized tapered optical fiber structure can accurately measure magnetic fields in the range of 5–600 mT, whereas the preoptimized (W/O MGO-coated) tapered optical fiber structure can only accurately measure magnetic fields in the range of 50–350 mT, as shown in Fig. 11. And it is evident that the wavelength shift of the tapered fiber optic structure prior to optimization is small under magnetic fields of varying field strengths, and the measurement accuracy is low. Clearly, the prepared MGO-coated tapered fiber-optic structures are capable of wide-range, high-precision measurements of magnetic fields. Figs. 12 and 13 depict the wavelength shift of light in the fiber under increasing and decreasing magnetic fields, respectively. It occurs due to changes in the RI of

the MGO resulting from changes in the core and cladding modes of the tapered fiber. In the normalized images of Figs. 12(a) and 13(a), wavelength shifts caused by varying magnetic field strengths are clearly visible. Wherein the fiber optic probe has a sensitivity of 0.9 pm/mT and an accuracy of 0.9777 in an increasing magnetic field, as shown in Fig. 12(b), while the proposed sensor probe has a sensitivity of 1.6 pm/mT and an accuracy of 0.9866 in a decreasing magnetic field, as shown in Fig. 13(b).
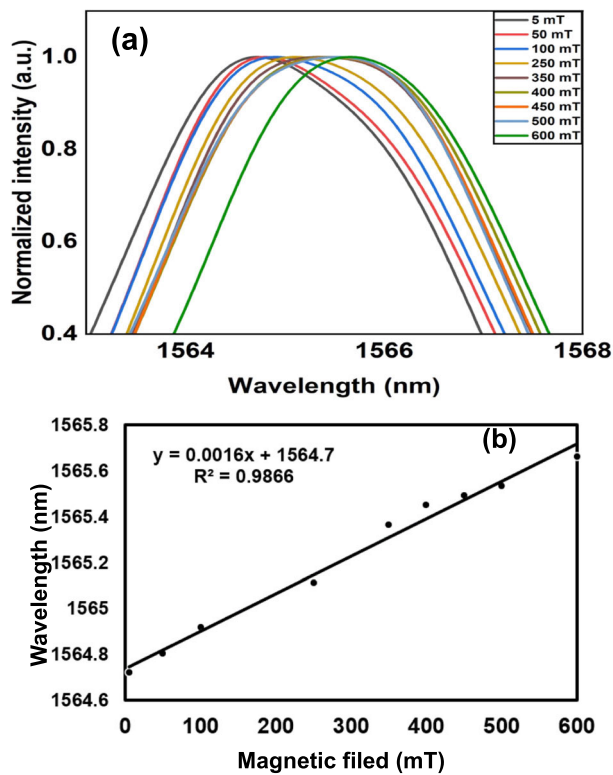
Fig. 13. Measurement of magnetic field (during decrease in magnetic field) utilizing the proposed SMF-based MGO-coated tapered fiber structure (a) sensing spectrum and (b) linear plot of the proposed sensor.

TABLE I
COMPARISON OF THE PROPOSED SENSOR'S PERFORMANCE DURING
FORWARD AND REVERSE MAGNETIC FIELD SENSING

Parameters	Forward sensing	Reverse sensing
Detection range	5-600 mT	5-600 mT
sensitivity	0.9 pm/mT	1.6 pm/mT
Accuracy	0.9777	0.9866

Table I shows the performance comparison of the proposed sensor during forward and reverse magnetic field sensing. According to the information in the Table I, we can speculate that the detection range of this sensor in both increasing and decreasing magnetic field can reach 5–600 mT. In increasing magnetic field, the sensitivity of this magnetic field sensor is 0.9 pm/mT, and its accuracy is 0.9777, but in decreasing magnetic field, its sensitivity is higher than that of increasing magnetic field to reach 1.6 pm/mT, and the accuracy can reach 0.9866; it is obvious that this magnetic field sensor has a good performance in decreasing magnetic field. It can also conclude that the magnetic field sensor has good performance in decreasing magnetic field. It has been observed that performance of reverse sensing of magnetic field detection is quite better than the forward sensing.

Table II organizes the nanomaterials used for magnetic field detection and performance comparison of proposed sensor with the existing sensors. By comparing the sensitivity and

TABLE II
VARIOUS MAGNETIC COATING MATERIALS AND PERFORMANCE
COMPARISON OF MAGNETIC FIELD SENSORS

Materials used	Sensing range	Sensitivity	Ref.
Magnetic fluid	2.6-24.8 mT	11.67 nm/mT	[23]
Ferrofluids	0 -140 Oe	−0.1130 dB/Oe	[24]
Ferromagnetic nanoparticles	40-1600 e	−0.1039 dB/Oe	[25]
MGO	5-600 mT	0.9 pm/mT 1.6 pm/mT	This Work

measurement range of the various materials-based sensors, we have observed that the MGO material used in this experiment has wide measurement range and better sensing performance in both increasing and decreasing magnetic fields, and it also shows good maneuverability in terms of the range of magnetic fields it can detect.

IV. CONCLUSION

The main objective of this work was to show the detailed fabrication of a tapered fiber optic sensor for measurement of wide range of magnetic fields. The fabricated tapered fiber optic structure is highly reproducible based on the experimental results. In this experiment, optimized the tapered fiber structure by coating the fiber's sensing region with MGO and measuring wavelength offsets in the presence of magnetic fields of increasing and decreasing strength. The sensitivity of the developed probe is 0.9 and 1.6 pm/mT in increasing and decreasing magnetic fields, respectively. The experimental results demonstrate that the tapered fiber optic structure has a high degree of accuracy and sensitivity in magnetic fields with changing trends. It is important to acknowledge that the magnetic field measurements were restricted to the range of 5–600 mT as a result of the constraints imposed by the experimental setup. If the magnetic field generator is capable of generating a greater magnetic field, it is expected that the magnetic field sensor will detect a bigger magnetic field strength while still maintaining satisfactory stability. Therefore, the novel sensor probe proposed in this work has an important potential for application in the field of noninvasive magnetic field measurements in various industries.

REFERENCES

[1] J. Chen, S. Althaus, H. Zhang, and M. Boudjatit, "Automatic high-spatial-resolution nuclear-magnetic-resonance spectroscopy and imaging system for rock cores," *Microsc. Microanal.*, vol. 27, no. S1, pp. 3286–3289, Aug. 2021, doi: 10.1017/S1431927621011314.

[2] Z. Jiang et al., "High-sensitivity vector magnetic field sensor based on side-polished fiber plasmon and ferrofluid," *Opt. Lett.*, vol. 43, no. 19, p. 4743, Oct. 2018, doi: 10.1364/OL.43.004743.

[3] C. Fischer, Q. Boehler, and B. J. Nelson, "Using magnetic fields to navigate and simultaneously localize catheters in endoluminal environments," *IEEE Robot. Autom. Lett.*, vol. 7, no. 3, pp. 7217–7223, Jul. 2022, doi: 10.1109/LRA.2022.3181420.

[4] H. Li, J. Qu, X. Jiang, and Y. Niu, "A correlation analysis of geomagnetic field characteristics in geomagnetic perceiving navigation," *Frontiers Neurorobotics*, vol. 15, Dec. 2021, Art. no. 785563, doi: 10.3389/fnbot.2021.785563.

[5] D. Shi, M. E. Sadat, A. W. Dunn, and D. B. Mast, "Photo-fluorescent and magnetic properties of iron oxide nanoparticles for biomedical applications," *Nanoscale*, vol. 7, no. 18, pp. 8209–8232, 2015, doi: 10.1039/C5NR01538C.

[6] J. S. Kumar, P. S. Paul, G. Raghunathan, and D. G. Alex, "A review of challenges and solutions in the preparation and use of magnetorheological fluids," *Int. J. Mech. Mater. Eng.*, vol. 14, no. 1, p. 13, Dec. 2019, doi: 10.1186/s40712-019-0109-2.

[7] K. Královec et al., "Magnetic nanoparticles of Ga-substituted ε-Fe$_2$O$_3$ for biomedical applications: Magnetic properties, transverse relaxivity, and effects of silica-coated particles on cytoskeletal networks," *J. Biomed. Mater. Res. A*, vol. 108, no. 7, pp. 1563–1578, Jul. 2020, doi: 10.1002/jbm.a.36926.

[8] S. Amiri and H. Shokrollahi, "The role of cobalt ferrite magnetic nanoparticles in medical science," *Mater. Sci. Eng., C*, vol. 33, no. 1, pp. 1–8, Jan. 2013, doi: 10.1016/j.msec.2012.09.003.

[9] S.-W. Kim et al., "Studying the reduction of graphene oxide with magnetic measurements," *Carbon*, vol. 142, pp. 373–378, Feb. 2019, doi: 10.1016/j.carbon.2018.10.068.

[10] J. Guo, L. Gui, W. Hou, L. Sun, Y. Liu, and J. Li, "Quality study and numerical simulation analysis of solid–liquid two-phase magnetic fluid polishing seven-order variable-diameter pipe," *Micromachines*, vol. 13, no. 4, p. 500, Mar. 2022, doi: 10.3390/mi13040500.

[11] Y.-Z. Zhang, "A magnetic confinement nuclear fusion mechanism for solar flares," *Res. Astron. Astrophys.*, vol. 20, no. 2, p. 26, Mar. 2020, doi: 10.1088/1674-4527/20/2/26.

[12] A. G. Chiariello, A. Formisano, F. Ledda, R. Martone, and F. Pizzo, "A fast reconstruction approach for the assessment of magnetic diagnostic systems in nuclear fusion devices," *IEEE Trans. Magn.*, vol. 54, no. 3, pp. 1–4, Mar. 2018, doi: 10.1109/TMAG.2017.2771753.

[13] F. B. Mancoff, J. H. Dunn, B. M. Clemens, and R. L. White, "A giant magnetoresistance sensor for high magnetic field measurements," *Appl. Phys. Lett.*, vol. 77, no. 12, pp. 1879–1881, Sep. 2000, doi: 10.1063/1.1311316.

[14] J. Lenz and S. Edelstein, "Magnetic sensors and their applications," *IEEE Sensors J.*, vol. 6, no. 3, pp. 631–649, Jun. 2006, doi: 10.1109/JSEN.2006.874493.

[15] B. Maleki, F. Taheri, R. Tayebee, and F. Adibian, "Dendrimer-functionalized magnetic graphene oxide for knoevenagel condensation," *Organic Preparations Procedures Int.*, vol. 53, no. 3, pp. 284–290, May 2021, doi: 10.1080/00304948.2021.1875799.

[16] S. Hemmati, P. Mohammadi, A. Sedrpoushan, and B. Maleki, "Synthesis of 2,5-dimethyl-N-substituted pyrroles catalyzed by diethylenetriaminepentaacetic acid supported on Fe$_3$O$_4$ nanoparticles," *Organic Preparations Procedures Int.*, vol. 50, no. 5, pp. 465–481, Sep. 2018, doi: 10.1080/00304948.2018.1525668.

[17] G. Sharma, A. M. Shrivastav, A. Jana, and R. Jha, "Synthesized Fe$_3$O$_4$ nanoflowers coated microfiber as magnetometer," *IEEE Photon. Technol. Lett.*, vol. 30, no. 22, pp. 1925–1928, Nov. 15, 2018, doi: 10.1109/LPT.2018.2872592.

[18] S. Khamari, A. Kumar, N. Mohapatra, and R. Jha, "Nickel ferrite nano fluid functionalized tapered microfiber based magnetometer," *J. Phys., Conf. Ser.*, vol. 2426, no. 1, Feb. 2023, Art. no. 012018, doi: 10.1088/1742-6596/2426/1/012018.

[19] N. Agrawal et al., "Detection of L-cysteine using silver nanoparticles and graphene oxide immobilized tapered SMS optical fiber structure," *IEEE Sensors J.*, vol. 20, no. 19, pp. 11372–11379, Oct. 2020, doi: 10.1109/JSEN.2020.2997690.

[20] Y. Tian, W. Wang, N. Wu, X. Zou, and X. Wang, "Tapered optical fiber sensor for label-free detection of biomolecules," *Sensors*, vol. 11, no. 4, pp. 3780–3790, Mar. 2011, doi: 10.3390/s110403780.

[21] Y. He, C. Yi, X. Zhang, W. Zhao, and D. Yu, "Magnetic graphene oxide: Synthesis approaches, physicochemical characteristics, and biomedical applications," *TrAC Trends Anal. Chem.*, vol. 136, Mar. 2021, Art. no. 116191, doi: 10.1016/j.trac.2021.116191.

[22] T.-Y. Gao et al., "Effect of structure on sensitivity of magnetic field sensor based on non-adiabatic tapered optical fiber with magnetic fluid," *IEEE Sensors J.*, vol. 22, no. 5, pp. 4022–4027, Mar. 2022, doi: 10.1109/JSEN.2022.3142313.

[23] Z. Hao, Y. Li, S. Pu, J. Wang, F. Chen, and M. Lahoubi, "Ultrahigh-performance vector magnetic field sensor with wedge-shaped fiber tip based on surface plasmon resonance and magnetic fluid," *Nanophotonics*, vol. 11, no. 15, pp. 3519–3528, Aug. 2022, doi: 10.1515/nanoph-2022-0224.

[24] S. Duan et al., "Intensity-interrogated magnetic sensor based on S-tapered and multimode fiber integrated with ferrofluids," *Appl. Opt.*, vol. 60, no. 34, p. 10743, Dec. 2021, doi: 10.1364/AO.443630.

[25] J. Zhang et al., "All-fiber magnetic field sensor based on tapered thin-core fiber and magnetic fluid," *Appl. Opt.*, vol. 56, no. 2, p. 200, Jan. 2017, doi: 10.1364/AO.56.000200.

Qianyun Yin is pursuing the bachelor's degree in optoelectronic information science and engineering with the Ji Xianlin College and the School of Physics Science and Information Technology, Liaocheng University, Liaocheng, China.

Her research interests include optical fiber sensors and magnetometers.

Ragini Singh received the Ph.D. degree from Ahmedabad University, Ahmedabad, India, in 2018.

She is currently working as an Assistant Professor with the School of Agriculture Science, Liaocheng University, Liaocheng, China. Her research interests include nanotechnology, molecular biology, environmental biology, and immunology.

Dr. Singh is a Lifetime Member of Materials Research Society of India and Indian Society of Nanomedicine. She is an Active Reviewer of *Three-Biotech*, *Biosensors and Bioelectronics*, IEEE SENSORS JOURNAL, and *Biomedical Optics Express*.

Bingyuan Zhang received the Ph.D. degree from the Beijing University of Technology, Beijing, China, in 2008.

He is currently working as a Professor with Liaocheng University, Liaocheng, China. He has authored more than 150 high-quality of research articles in his research domain. His research interests include experimental physics, lasers, and optical fiber-based biosensors.

Santosh Kumar (Senior Member, IEEE) received the Ph.D. degree from the Indian Institute of Technology (Indian School of Mines) Dhanbad, Dhanbad, India, in 2014.

He is an OPTICA Traveling Lecturer. He is currently a Professor with the School of Physics Science and Information Technology, Liaocheng University, Liaocheng, China. He has been supervised 12 M.Tech. dissertations and six Ph.D. candidates. He has authored more than 310 high-quality research articles in national and international SCI journals and conferences. He has presented numerous articles at conferences held in China, India, Belgium, and USA. He has recently published two scholarly books *2-D Materials for Surface Plasmon Resonance-Based Sensors* (CRC Press, 2021) and *Optical Fiber-Based Plasmonic Biosensors: Trends, Techniques, and Applications* (CRC Press, 2022). He has reviewed over 1800 SCI journals published by IEEE, Elsevier, Springer, OPTICA, SPIE, Wiley, ACS, and Nature up to this point. His current research interests include optical fiber sensors, waveflex sensors, nano and biophotonics, photonic and plasmonic devices, and waveguides and interferometers.

Dr. Kumar is a Fellow of SPIE and a Senior Member of SPIE and OPTICA. He is also the Chair of the OPTICA Optical Biosensors Technical Group. He has given numerous invited talks and serves as the session chair for IEEE Conferences. He has received the "2022 Best Performing Associate Editor" Award from IEEE SENSORS JOURNAL. He has served as an Associate Editor for IEEE SENSORS JOURNAL, IEEE INTERNET OF THINGS, and *Biomedical Optics Express*.